JACS
JOURNAL OF THE AMERICAN CHEMICAL SOCIETY

pubs.acs.org/JACS

Article

Unraveling the Pivotal Role of Atropisomerism for Cellular Internalization

Claire Donohoe, Fábio A. Schaberle, Fábio M. S. Rodrigues, Nuno P. F. Gonçalves, Christopher J. Kingsbury, Mariette M. Pereira, Mathias O. Senge, Lígia C. Gomes-da-Silva,* and Luis G. Arnaut*

Cite This: *J. Am. Chem. Soc.* 2022, 144, 15252−15265

Read Online

ACCESS | Metrics & More | Article Recommendations | Supporting Information

ABSTRACT: The intrinsic challenge of large molecules to cross the cell membrane and reach intracellular targets is a major obstacle for the development of new medicines. We report how rotation along a single C−C bond, between atropisomers of a drug in clinical trials, improves cell uptake and therapeutic efficacy. The atropisomers of redaporfin (a fluorinated sulfonamide bacteriochlorin photosensitizer of 1135 Da) are separable and display orders of magnitude differences in photodynamic efficacy that are directly related to their differential cellular uptake. We show that redaporfin atropisomer uptake is passive and only marginally affected by ATP depletion, plasma proteins, or formulation in micelles. The α_4 atropisomer, where *meso*-phenyl sulfonamide substituents are on the same side of the tetrapyrrole macrocycle, exhibits the highest cellular uptake and phototoxicity. This is the most amphipathic atropisomer with a conformation that optimizes hydrogen bonding (H-bonding) with polar head groups of membrane phospholipids. Consequently, α_4 binds to the phospholipids on the surface of the membrane, flips into the membrane to adopt the orientation of a surfactant, and eventually diffuses to the interior of the cell (bind-flip mechanism). We observed increased α_4 internalization by cells of the tumor microenvironment in vivo and correlated this to the response of photodynamic therapy when tumor illumination was performed 24 h after α_4 administration. These results show that properly orientated aryl sulfonamide groups can be incorporated into drug design as efficient cell-penetrating motifs in vivo and reveal the unexpected biological consequences of atropisomerism.

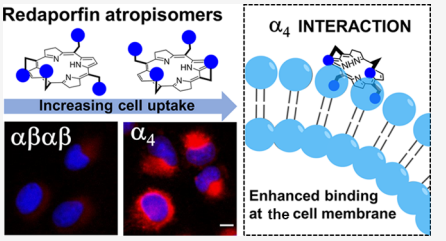

INTRODUCTION

The outer membrane of mammalian cells severely restricts the uptake of large molecules (>1000 Da) by passive diffusion. This is a major barrier in drug development and has motivated the development of membrane-anchoring moieties to enhance membrane interaction[1] as well as cell-penetrating motifs to unlock macromolecule cytosolic delivery.[2−8] It is reasonably established that such motifs must be amphipathic in order to disrupt the interface between the bilayer membrane core and the extracellular aqueous phase.[4,9] Additionally, they should reduce the energy penalty of transition from this aqueous phase to a lipophilic membrane.[10,11] A good example of a cell-penetrating motif is the guanidinium group anchored to an aromatic hydrophobic scaffold. This may form bidentate bonds with sulfates and carboxylates of the cell surface and promote cell internalization.[2,9,12] Interestingly, the higher phototoxicity of photosensitizers for photodynamic therapy (PDT) of cancer bearing guanidinium groups was deemed to be a result of higher cell uptake.[13] Although many advances in macromolecule cell uptake have been achieved, useful structure−function relationships are still lacking, and macromolecule delivery to any and all cells in the body remains a major unmet need.

Atropisomers are separable conformers with hindered rotation along a single bond, which becomes a source of axial chirality when asymmetric substitution about the bond is present. Distinctively, conversion between stereoisomers at high temperatures occurs by rotation of a single bond, rather than by bond-breaking−bond-forming processes. Conformers are regarded as atropisomers when their interconversion at room temperature occurs with a half-life >1000 s, which usually corresponds to a barrier height for rotation >20 kcal mol^{-1}.[14−19] Atropisomerism, although frequently disregarded, is a useful method to introduce structural diversity in drug design and increase target selectivity. Examples of atropisomers are pervasive in kinase inhibitors where ∼80% of FDA-approved kinase inhibitors contain at least one rapidly interconverting axis of atropisomerism.[18] Differential activities (potency and selectivity) were recently reported for atropisomers of pyrrolopyrimidine-based kinase inhibitors,

Received: June 2, 2022
Published: August 12, 2022

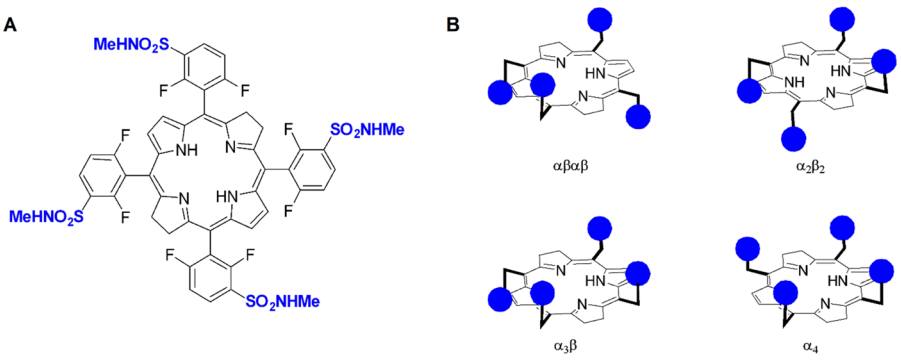

Figure 1. Redaporfin is a mixture of four atropisomers. (A) Redaporfin (i.e., 5,10,15,20-tetrakis(2,6-difluoro-3-*N*-methylsulfamoylphenyl)-bacteriochlorin), molecular weight 1135 Da. (B) Atropisomers: $\alpha\beta\alpha\beta$—two sulfonamides are on each side of the plane but in alternate positions; $\alpha_2\beta_2$—two sulfonamides on each side of the plane and adjacent to each other; $\alpha_3\beta$—three sulfonamides on the same side of the plane and one on the opposite side; α_4—all sulfonamides on the same side of the macrocycle plane.

where one form binds to the desired molecular target, while the other causes off-target effects by interfering with other kinases.[20] Current knowledge tends to limit the scope of differential atropisomer activity to distinct interactions of the separable conformers with their targets. It would not be expected that loose interactions of atropisomers with cell membranes would lead to differential activity. Nevertheless, we show here for the first time that atropisomers of a photosensitizer in phase I/II clinical trials for head and neck cancer (NCT02070432),[21] named redaporfin (Figure 1), have dramatically different pharmacological performances and relate such differences to cell uptake.

PDT employs a photosensitizer molecule, light of a specific wavelength absorbed by the photosensitizer, and molecular oxygen to induce a therapeutic effect. The photosensitizer acts like a pro-drug because it is activated by light. The electronically excited photosensitizer transfers its excess energy to molecular oxygen to generate singlet oxygen or is involved in electron transfer processes which generate additional reactive oxygen species (ROS).[22−25] The local oxidative stress caused by ROS triggers cell death in the field of illumination, as well as systemic anti-tumor immune responses, which contribute to long-term control of cancer.[26] The most frequently used photosensitizers are porphyrin derivatives, including chlorins and bacteriochlorins.[27,28] The availability of robust synthetic methods to prepare large quantities of *meso*-arylporphyrin derivatives[29,30] has promoted the synthesis of a variety of photosensitizers with macrocycle-aryl bonds which exhibit atropisomerism. Large substituents in phenyl *ortho* positions hinder rotation around the macrocycle-aryl bond, and the asymmetry of the substitution generates atropisomers.[31] The structures of these tetrapyrrole photosensitizers were originally referred to as "picket-fence". The biological relevance of these "picket-fence" systems has been typically reserved as model complexes for dioxygen binding to heme.[32]

Atropisomers of *meso*-arylporphyrin derivatives investigated as PDT photosensitizers have been isolated and characterized.[33−37] Isomers with similar photophysical properties are expected to give similar ROS quantum yields because neither energy nor electron transfer reactions require close contact with oxygen.[38] Hence, conventional wisdom is that individual photosensitizer isomers should display similar behavior as isomer mixtures. This was observed with benzoporphyrin derivative monoacid ring A (named verteporfin), which has two regioisomers with similar phototoxicity.[39] Both isomers are present in Visudyne for the PDT of age-related macular degeneration. Increased photoactivity of a specific atropisomer has only been reported for a more polar atropisomer with higher propensity for differential monomeric solubilization in aqueous solutions[33] and for structural isomers with large differences in polarity (or in the logarithm of the *n*-octanol:water partition coefficient, $\mathrm{LogP_{OW}}$) which cause differences of cellular uptake.[40,41]

Redaporfin is a photostable bacteriochlorin photosensitizer with simple synthesis, intense absorption at 749 nm, and high ROS yield,[23,42−44] which has exhibited high cure rates in different mouse models of cancer (e.g., CT26, B16-F10, S91, and LLC cancer cells), including abscopal inhibition of metastasis outside of the field of illumination.[44−49] A fluorine substituent in an *ortho* position of a phenyl group is not sufficient to hinder phenyl-macrocycle bond rotation to yield separable atropisomers at room temperature,[50] but we show here that fluorine substituents in both *ortho* positions of redaporfin phenyl groups and their sulfonamide groups lead to atropisomers with configurational stability of years at room temperature. We separated four atropisomers—$\alpha\beta\alpha\beta$, $\alpha_2\beta_2$, $\alpha_3\beta$, and α_4—which differ by the spatial orientation of the sulfonamide groups with respect to the macrocycle (Figure 1B).[51] Although the chemical properties of the atropisomers are remarkably similar, their biological activities differ by orders of magnitude. We show that the PDT efficacies of atropisomers are related to their ability to diffuse across the cell membrane. This reveals unsuspected consequences of atropisomerism in cell uptake. The spatial orientation of polar substituents has profound consequences in cellular uptake and opens new perspectives for cytosolic delivery of large molecules.

RESULTS AND DISCUSSION

Redaporfin Atropisomers Are Separable and Stable at Room Temperature. Redaporfin (and related chlorin and porphyrin derivatives)[43] atropisomers were initially separated by semi-preparative HPLC at room temperature.[51] This time-consuming process was advantageously replaced by reversed-phase (RP) flash chromatography. Rapid and efficient separation of the redaporfin atropisomers was possible using a RP silica gel C18 column with an increasing gradient of acetonitrile in water (60−90% MeCN) at T = 23 °C for 90 min. This was followed by acetonitrile evaporation under

https://doi.org/10.1021/jacs.2c05844
J. Am. Chem. Soc. 2022, 144, 15252−15265

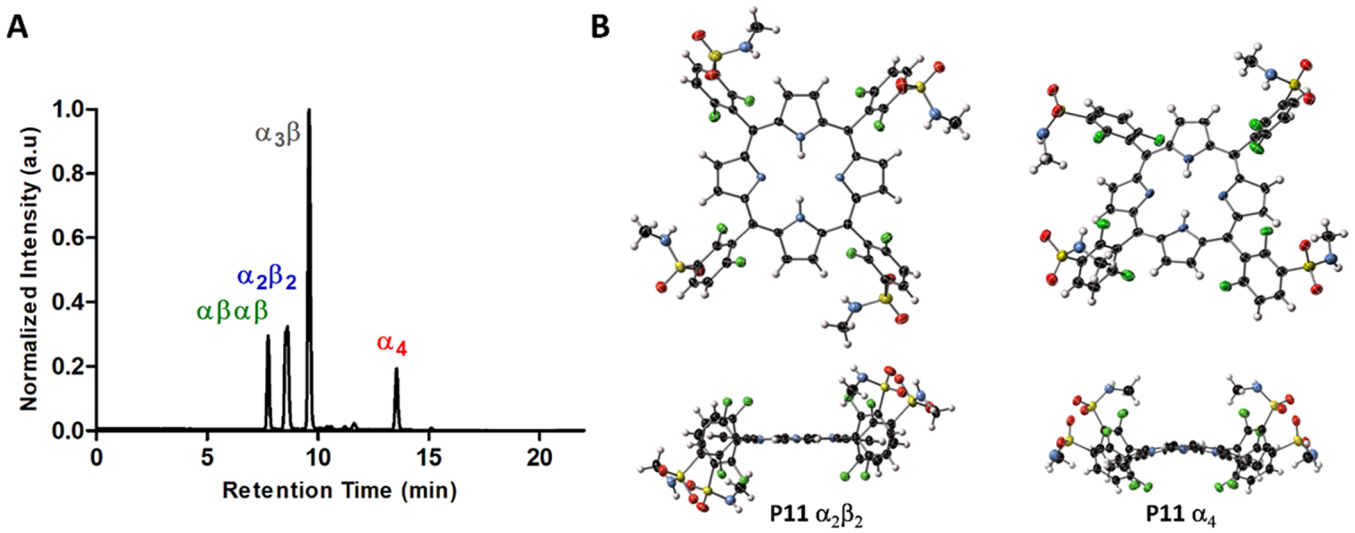

Figure 2. Separation and X-ray crystal structures of redaporfin atropisomers. (A) Representative RP-HPLC chromatogram of redaporfin where the individual atropisomers were detected by absorption at 743 nm. (B) View of the molecular structure in the crystal of $\alpha_2\beta_2$ and α_4 atropisomers of P11, where the $\alpha_2\beta_2$ and the α_4 atropisomers were obtained from $\alpha_2\beta_2$·2Me$_2$SO and α_4·4MeCN, respectively (ellipsoids are shown at the 50% probability level, and H-atoms are represented as spheres of fixed radius).

vacuum (maintaining pressure at 220 mbar and T < 40 °C) and water removal by lyophilization. Each fraction was evaluated for atropisomeric purity by RP-HPLC and ^{1}H NMR (Figures 2A and S1). The retention times of the atropisomers of redaporfin and the corresponding precursor porphyrins (named P11) were similar (Figures 2A and S2). Fractions of atropisomeric purity (~90%), confirmed by RP-HPLC, were used for photochemical, photophysical, and biological evaluations. The RP-HPLC of redaporfin indicates that the α_4 atropisomer accounts for the lowest proportion of the mixture (~13%) followed by $\alpha\beta\alpha\beta$ (~14%), $\alpha_2\beta_2$ (~24%), and $\alpha_3\beta$ (~49%), which is consistent with their expected statistical abundance, 1:1:2:4.[32] Redaporfin is the statistical mixture of atropisomers.

It is important to emphasize that the order of RP-HPLC retention times in Figure 2A is the same as the order of R_f (retention factor) values of atropisomers separated by silica gel thin-layer chromatography and in silica gel columns using ethyl acetate: dichloromethane (20:1 v/v followed by 3:2 v/v) as the eluent.[51] The assignment in Figure 2A does not follow the conventional expectation that α_4, with all dipole moments of polar groups pointing to the same side of the macrocycle, should be the most polar atropisomer. Typically, the more polar atropisomer should have the highest retention time in silica gel chromatography and the lowest retention time in RP-HPLC. It was, therefore, unexpected that α_4 was observed to have the highest chromatographic retention time regardless of the choice of stationary phase. The order of atropisomer elution was the same as that of the silica gel (ethyl acetate:dichloromethane as the eluent) or a RP silica gel, hydrophobic octadecylsilane (C18) column (acetonitrile:water as the eluent). The retention factors of drugs in a C18 column, with acetonitrile:water used as a mobile phase, generally correlates with lipophilicity and LogP_{OW}.[52] α_4 shows a greater affinity for hydrophobic C18 in the stationary phase than for the polar eluent. Thus, the higher retention factor of α_4 in RP-HPLC suggests that it is the most lipophilic atropisomer, whereas its higher retention in normal phase silica gel column chromatography can be attributed to stronger hydrogen bonding of its four sulfonamide groups with silanol (SiOH) groups on the surface of silica. Together, these results demonstrate the strong amphipathic character of α_4.

Crystals were grown from the fractions assigned to $\alpha_2\beta_2$ and α_4 P11 atropisomers, and their molecular structures determined by X-ray diffraction studies. Modeling of diffraction data unambiguously confirmed structure assignment, with the identified atropisomer as the sole component of each structure (Figures 2B and S3−S6, Table S1). Hydrogen bonding of the sulfonamide moiety is the most prominent of intermolecular interactions in each case. The $\alpha_2\beta_2$ P11 atropisomer interacts with the DMSO solvate through the N−H protons on the sulfonamide group (2.825(7) Å N···O) and with sulfonamide groups of adjacent molecules (3.036(16) Å N···O). One of these sulfonamide groups exhibits minor conformational disorder (Figure S3C). In the $\alpha_2\beta_2$ atropisomer, the porphyrin core adopts a primarily planar modality with localized H-atoms. Consistent with the $\alpha_2\beta_2$ atropisomerism, inversion symmetry exists at the center of the molecule; aryl rings are inclined at 76° and 64° to the mean plane of the porphyrin (Figures 2B and S3A−D), as expected for *ortho*-substituted 5,10,15,20-tetraarylporphyrins. In contrast, the α_4 P11 atropisomer (α_4·1·4MeCN) does not interact strongly with the included solvate; H-bonding networks of porphyrins define channels of 17% of the crystal volume, which are filled with disordered MeCN (Figures 2B and S4).[53] Individual α_4 P11 atropisomers are linked together by N−H···O bonding (2.984(13) and 3.020(12) Å N···O) between proximal sulfonamide groups, thus forming a three-dimensional hydrogen-bonded lattice (Figures S3E−G and S4). Overlay of these structures with the CuTPP reference compound (Figures S5−6) reveals isotropic expansion of the porphyrin core relative to the reference, expected for free base porphyrins.[54] The α_4 structure shows out-of-plane deformation, primarily of the saddle type and similar in magnitude to the most distorted heme B subunits in protein structures.[55] The NSD values for both atropisomers are shown in Figures S5C and S6C.

In view of the nonintuitive retention factors of silica gel and RP-HPLC, we evaluated the relative "polarity" of the

https://doi.org/10.1021/jacs.2c05844
J. Am. Chem. Soc. 2022, 144, 15252−15265

Table 1. Photophysical and Photochemical Properties of Redaporfin Atropisomers

sample	λ_{max},[a] nm	ε_{max},[a] mM^{-1} cm^{-1}	τ_T,[a] ns	Φ_{PD},[b] $/10^{-6}$	Φ_Δ[a]	Φ_F[a]	$LogP_{OW}$
redaporfin[43]	743	140	216	10	0.43	0.138	1.9
$\alpha\beta\alpha\beta$	743	126	257	15	0.39	0.182	2.6
$\alpha_2\beta_2$	743	137	296	15	0.35	0.201	2.6
$\alpha_3\beta$	743	137	268	12	0.50	0.206	3.3
α_4	743	122	266	9	0.49	0.171	2.9

[a]In ethanol. [b]In methanol:PBS, 3:2.[51]

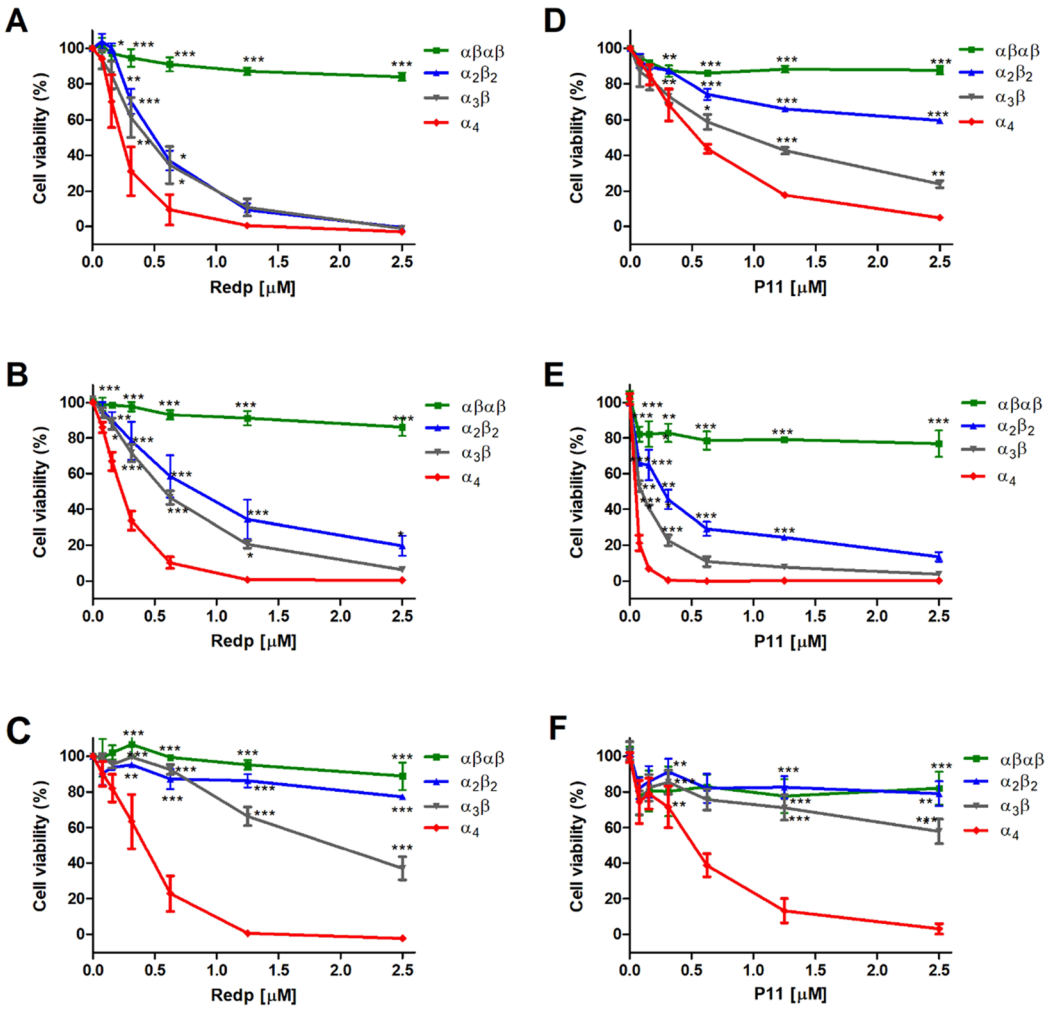

Figure 3. Phototoxicities of redaporfin atropisomers and of P11 atropisomers upon illumination at 740 nm (0.2 J/cm^2) or 410 nm (0.0125 or 0.05 J/cm^2), respectively, after 24 h of incubation. (A−C) U-2 OS, 4T1, and CT26 cells treated with redaporfin atropisomers. (D) U-2 OS cells treated with P11 atropisomers and 0.0125 J/cm^2. (E−F) 4T1 and CT26 cells treated with P11 atropisomers and 0.05 J/cm^2. Dose−response curves indicate the mean ± SEM of 2−3 independent experiments. Statistical significance was evaluated using two-way ANOVA vs the α_4 atropisomer, * $p < 0.05$, ** $p < 0.01$, and *** $p < 0.001$.

atropisomers dissolving the P11 atropisomer mixture in dichloromethane, combined with an equal volume of hexane. The solvent mixture is less polar than the initial solvent (dichloromethane) and a fraction of P11 precipitates (fraction *X*). The fraction remaining in the solvent mixture was recovered by solvent evaporation (fraction *Y*). RP-HPLC of P11, fraction *X*, and fraction *Y* reveals that the content of α_4 is higher in fraction *Y* than in fraction *X*. This means that α_4 is more soluble in the less polar solvent mixture and may be regarded as the most lipophilic atropisomer (Figure S7 and Table S4), although it is also the atropisomer that binds more strongly to silica gel, thereby further indicating an amphipathic character.

The rates of interconversion of the atropisomers were studied at 140 °C in dimethylformamide starting with 99% of the $\alpha_3\beta$ atropisomer (Table S5).[51] The content of $\alpha_3\beta$ was reduced from 99% at $t = 0$ to 60% in 5 min, 58% in 10 min, and 52% in 20 min. At $t = 20$ min, all atropisomers nearly recovered their proportions in the statistical mixture. Applying relaxation kinetics, this corresponds to a relaxation time ∼4 min at 140 °C. A similar experiment at 85 °C gave a relaxation time ∼1000 min, which leads to a barrier height for bond

https://doi.org/10.1021/jacs.2c05844
J. Am. Chem. Soc. 2022, 144, 15252−15265

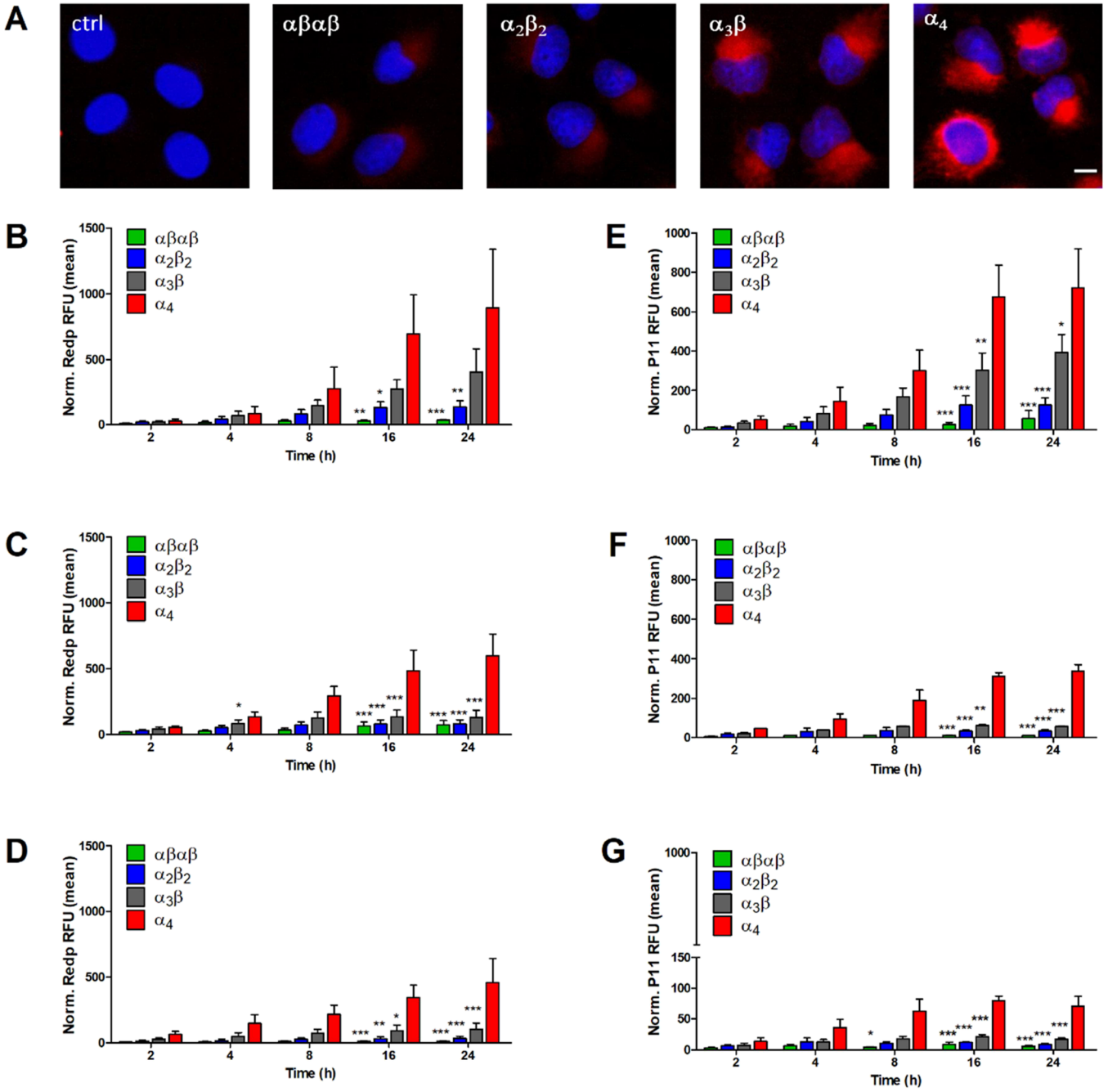

Figure 4. Cell uptake of redaporfin and P11 atropisomers at different incubation times. (A) Fluorescence from U-2 OS cells incubated with redaporfin atropisomers (red) for 24 h, followed by nucleus staining with DAPI (blue); scale bar = 10 μm. (B–D) Cellular internalization of redaporfin atropisomers evaluated by flow cytometry at the indicated time points in U-2 OS, 4T1, and CT26 cells. (E–G) Cellular internalization of P11 atropisomers evaluated by flow cytometry at the indicated time points in U-2 OS, 4T1, and CT26 cells; bars indicate the mean ± SEM of 2–3 independent experiments; the fluorescence signal from treated cells was normalized to the untreated cells; the statistical significance was evaluated using two-way ANOVA vs the α_4 atropisomer, * $p < 0.05$, ** $p < 0.01$, and *** $p < 0.001$.

rotation ~29 kcal mol^{-1}. The conversion between redaporfin atropisomers at room temperature is remarkably slow.

Redaporfin and P11 Atropisomers Have Similar Photophysical and Photochemical Properties. Redaporfin and its related atropisomers have very similar absorption spectra (Figure S8). Their infrared absorption maxima (λ_{max}) and corresponding molar absorption coefficients (ε_{max}) are presented in Table 1. The triplet decays are monoexponential with atropisomer triplet lifetimes (τ_T) in the 250–300 ns range in aerated solutions. Photodecomposition studies, evaluated through photobleaching experiments involving irradiation of the bacteriochlorins in methanol:PBS (3:2), indicate that α_4 (photodecomposition quantum yield $\Phi_{PD} = 9 \times 10^{-6}$) is slightly more photostable than the other atropisomers. Singlet oxygen emissions followed monoexponential decays and their intensities relative to a reference allowed for the determination of singlet oxygen quantum yields (Φ_Δ). The Φ_Δ values obtained for the $\alpha_3\beta$ and α_4 atropisomers are higher than for the other atropisomers. The fluorescence quantum yields (Φ_F) of all atropisomers are reasonably similar. The differences in

https://doi.org/10.1021/jacs.2c05844
J. Am. Chem. Soc. 2022, 144, 15252–15265

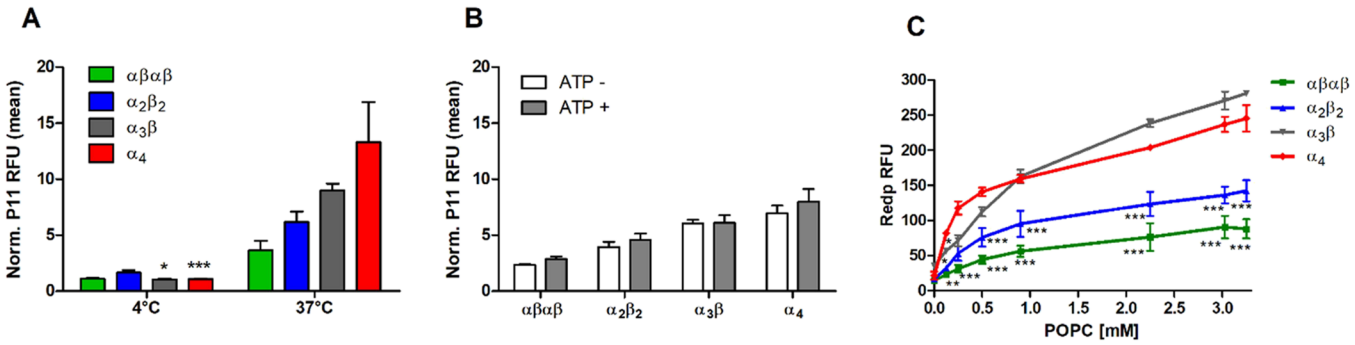

Figure 5. Mechanism of atropisomer internalization in 4T1 cells. (A) P11 atropisomers (2.5 μM) incubated for 4 h at 4 °C or 37 °C or (B) incubated for 2 h upon ATP depletion; bars indicate the mean ± SEM of 2 or 3 independent experiments. (C) Fluorescence of redaporfin atropisomers (5 μM) after 20 min incubation with various concentrations of POPC liposomes; each point is mean ± SEM of 2 independent experiments; statistical significance was evaluated using two-way ANOVA vs the α_4 atropisomer, * $p < 0.05$, ** $p < 0.01$, and *** $p < 0.001$.

photophysical/photochemical properties of the atropisomers are small and tend to compensate each other. For example, while α_4 is slightly more photostable and its Φ_Δ is high, it also has the lowest ε_{max}. Based on these properties, all atropisomers should have very similar PDT efficacies. Table 1 also presents $LogP_{OW}$ values obtained with a modification of the shake-flask method. Interestingly, the higher lipophilicity of α_4, revealed with the addition of hexane to dichloromethane, is not reflected in its $LogP_{OW}$ value. The observed high amphipaticity of α_4 defies classifications of "polarity" or "lipophilicity".

Redaporfin Atropisomers Have Very Different Phototoxicities. Similar to the redaporfin mixture, individual atropisomers do not show cytotoxicity in the dark, up to at least 20 μM (Figure S9A). The same applies to P11 atropisomers (Figure S9B). Surprisingly, the phototoxicity of isolated atropisomers may differ by orders of magnitude for the same light dose (Figure 3). For example, 0.2 μM of α_4 killed 50% of U-2 OS cells with a light dose of 0.2 J/cm^2 at 740 nm, whereas the phototoxicity of $\alpha\beta\alpha\beta$ with the same light dose remained negligible at 2.5 μM. The same order of phototoxicity, α_4 (high phototoxicity) > $\alpha_3\beta$ > $\alpha_2\beta_2$ > $\alpha\beta\alpha\beta$ (low phototoxicity), was observed in all cancer cell lines investigated in this work [human bone osteosarcoma (U-2 OS), mouse mammary gland breast cancer (4T1), and mouse colon carcinoma (CT26)].

Similar results were obtained with the P11 porphyrin atropisomers (Figures 3D−F and S9C), although the light dose which revealed differential phototoxicity in U-2 OS cells (0.0125 J/cm^2) had to be lower than for CT26 and 4T1 cells (0.05 J/cm^2). Of note, the viability of U-2 OS cells incubated with 1 μM of the $\alpha\beta\alpha\beta$ P11 atropisomer decreased by >90% after treatment with 0.05 J/cm^2 (Figure S9C). This showed that all atropisomers may be phototoxic, although this could require widely different drug and light doses. The photophysical and photochemical properties of redaporfin atropisomers cannot explain their differential phototoxicity; however, their order of phototoxicity is the same as their RP-HPLC retention times.

Redaporfin Atropisomers Differ in Their Ability to Passively Diffuse across Cell Membranes. Intrigued by the contrast between similar photochemical behavior and differential phototoxicity of redaporfin atropisomers, we investigated cell uptake in detail. Fluorescence microscopy showed that α_4 has a higher fluorescence intensity in U-2 OS cells after 24 h of incubation, followed by $\alpha_3\beta$, $\alpha_2\beta_2$, and finally by $\alpha\beta\alpha\beta$ (Figure 4A). The pattern of distribution is very similar to that reported for redaporfin, suggesting tropism for the endoplasmic reticulum and Golgi compartments.[56,57] This was further confirmed with P11 as all atropisomers demonstrated fluorescence overlap with GFP-CALR expressed in the endoplasmic reticulum and GFP-GALT1 expressed in the Golgi compartment (Figure S10). The kinetics of cell uptake were followed by flow cytometry at fixed incubation periods (2, 4, 8, 16, and 24 h) with the atropisomers (Figure 4B−G). Uptake of all atropisomers increased over time, but their relative intracellular concentrations were maintained: α_4 > $\alpha_3\beta$ > $\alpha_2\beta_2$ > $\alpha\beta\alpha\beta$. After 24 h of incubation, 10- to 40-fold increase of cellular internalization was attained for the α_4 atropisomer when compared to the $\alpha\beta\alpha\beta$ counterpart. These findings were confirmed using an alternative method based on the lysis of cells, preincubated with the atropisomers for 24 h. Measurement of redaporfin or P11 fluorescence from the supernatant of cells confirmed the order of atropisomer internalization (Figure S11).

The order of increasing cell uptake in Figure 4 is the same as the order of phototoxicity in Figure 3. Moreover, U-2 OS cells exhibited the highest levels of atropisomer internalization (Figure 4B,E) and were the cells that also experienced the greatest response to PDT (Figure 3A,D). Conversely, CT26 cells showed the lowest internalization of the atropisomers (Figure 4D,G) and are more difficult to treat with PDT (Figure 3C,F). These results convincingly show that the phototoxicities of redaporfin and P11 atropisomers are directly related to their cell uptake. Thus, differential phototoxicity of atropisomers can be explained through understanding the differential uptake of the atropisomers, specifically why α_4 has enhanced internalization by the cells relative to $\alpha\beta\alpha\beta$. Remarkably, the order of retention in RP-HPLC is the same as the order of atropisomer cell uptake. For example, α_4 demonstrated the highest affinity to the column as well as enhanced internalization.

The lipophilicity of photosensitizers is widely accepted to correlate with their ability to diffuse across cell membranes and, consequently, to affect PDT efficacy.[58−61] The higher $LogP_{OW}$ of $\alpha_3\beta$ and α_4 might facilitate the interactions of these atropisomers with cell membranes (Table 1) but do not explain the superiority of α_4 compared to $\alpha_3\beta$. Additionally, $\alpha_2\beta_2$ exhibited a higher uptake than $\alpha\beta\alpha\beta$, although they have similar $LogP_{OW}$. Redaporfin and its $\alpha_3\beta$ atropisomer have similar uptakes (Figure S12), which can be explained, considering that ~50% of redaporfin is the $\alpha_3\beta$ atropisomer.

https://doi.org/10.1021/jacs.2c05844
J. Am. Chem. Soc. 2022, 144, 15252−15265

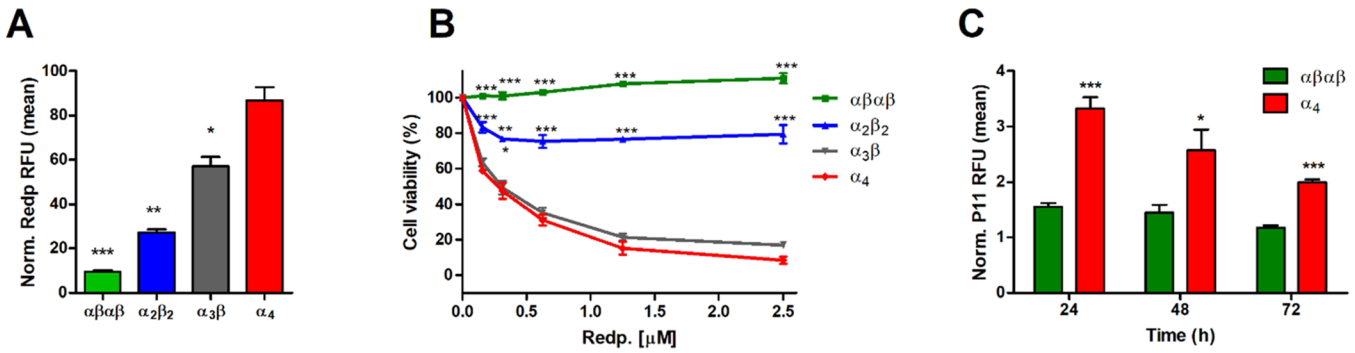

Figure 6. Atropisomer micelle formulation cell internalization. (A) Cellular internalization of redaporfin atropisomers in vitro formulated in Kolliphor EL assessed by flow cytometry after 24 h of incubation with 4T1 cells. Bars indicate mean ± SEM of 2 independent experiments; the statistical significance was evaluated using two-way ANOVA vs the α_4 atropisomer. (B) Phototoxicities of redaporfin atropisomers (formulated in Kolliphor EL) in vitro upon illumination at 740 nm (0.2 J/cm^2) after 24 h of incubation with 4T1 cells; statistical significance was evaluated using two-way ANOVA vs the α_4 atropisomer. (C) Level of internalization of α_4 and $\alpha\beta\alpha\beta$ P11 atropisomers in single cell suspensions obtained from CT26 tumors on female BALB/c at the indicated timepoints after i.v. administration, measured by flow cytometry; bars indicate the mean ± SEM of 4−5 mice; the fluorescence signal from treated cells was normalized to the untreated cells. Significance level of the difference between the two atropisomers was evaluated via unpaired *t*-test, $*p < 0.05$, $**p < 0.01$, and $***p < 0.001$.

Another factor that may interfere with the PDT efficacy of weakly soluble tetrapyrrole photosensitizers is a tendency to self-aggregate.[62] Planar macrocycles aggregate via strong interactions between adjacent π systems. Aggregated porphyrin derivatives have lower absorbance, lower fluorescence, shorter triplet lifetime, and lower singlet oxygen quantum yield. The interaction with the cell membranes and the mechanisms of cellular internalization are also different between aggregates and monomers.[63] Thus, self-aggregation of atropisomers may impact their performance.[60] We investigated P11 atropisomers in water with 0.4% DMSO and observed that the absorbance (Figure S13A) and emission (Figure S13B,C) spectra of all atropisomers were similarly quenched and broadened when compared to the molecules in pure DMSO. The fluorescence in DMSO/water was shifted in the same proportion for all atropisomers. In particular, the emission spectra of $\alpha\beta\alpha\beta$ and α_4 have similar bathochromic shifts (Figure S13C). This data indicates that atropisomer self-aggregation cannot explain the differences observed in cell uptake.

Next, we investigated the mechanism of atropisomer cellular internalization to obtain a better insight into α_4 enhanced uptake and PDT efficacy. Cell uptake rates, which increase dramatically with temperatures above 20 °C, are commonly associated with active mechanisms of transport requiring energy such as endocytosis.[64] Endocytosis is precluded at 4 °C,[65] and Figure 5A shows that α_4 cell uptake was significantly reduced but not entirely suppressed at 4 °C in comparison to 37 °C after 4 h of incubation. Passive permeation of the membrane is also dependent on the temperature as octanol−water partition coefficients are influenced by temperature.[58] Therefore, to clarify whether α_4 uptake was an active or passive process, we conducted uptake studies with depletion of ATP by means of 2-deoxy-D-glucose.[58,66] Our results showed that partial depletion of ATP (Figure S14A) had no significant impact on the uptake of all P11 atropisomers (Figure 5B), whereas, under the same conditions, inhibition of the recombinant GFP cell uptake (known to be energy-dependent)[67] was observed (Figure S14B). Thus, passive diffusion of the atropisomers and, in particular, of α_4, along a concentration gradient is the main mechanism responsible for the enhanced cell internalization.

Liposomes are useful models to predict the interactions of molecules with the cell membranes.[60,68] We incubated redaporfin atropisomers with increasing concentrations of 1-palmitoyl-2-oleoyl-*sn*-phosphatidylcholine (POPC) liposomes in PBS and measured atropisomer fluorescence intensities (Figure 5C) as an indicator of their interactions with phospholipid bilayer membranes. A stronger interaction will lead to more atropisomers present in the membrane where the molecules can disaggregate and yield monomers, which emit stronger fluorescence. The strong fluorescence of the α_4 atropisomer with small quantities of liposomes demonstrates that it strongly interacts with the membrane and disaggregates. It is very improbable that the atropisomers move from the bilayer membrane of the liposome to its aqueous compartment. This is not the case in cell uptake where the atropisomer may bind to lipophilic domains inside the cell and accumulate there. The increased cell uptake of α_4 can be understood on the basis of a strong affinity to phospholipid bilayer membranes, followed by fast crossing of the membrane and accumulation in the interior of the cell. The low uptake of $\alpha\beta\alpha\beta$ is clearly related to its weak interaction with lipidic membranes, at least to form fluorescent monomers. The results with low POPC concentrations are entirely consistent with the observed cell uptake. At high POPC concentrations, the $\alpha_3\beta$ atropisomer eventually becomes the most fluorescent atropisomer and the order of atropisomer incorporation in liposomes follows their $\mathrm{LogP_{OW}}$ values (Table 1). This is consistent with an approach to bulk properties when large POPC concentrations are present.

The interaction of photosensitizers with plasma proteins may alter cellular internalization, for example, by inhibiting passive diffusion and facilitating endocytic uptake. We investigated the impact of bovine serum albumin (BSA), high-density lipoprotein (HDL), and low-density lipoprotein (LDL) on atropisomer cellular uptake to identify challenges in the transfer from in vitro to in vivo studies. BSA and HDL (but not LDL) indistinctly enhanced the level of uptake for all atropisomers (Figure S15). Similar results have been described for other photosensitizers. For instance, LDL impaired porfimer sodium uptake, whereas BSA and HDL enhanced the cellular internalization of temoporfin and WST1.[69−72] Our results show that the presence of these plasma proteins

https://doi.org/10.1021/jacs.2c05844
J. Am. Chem. Soc. 2022, 144, 15252−15265

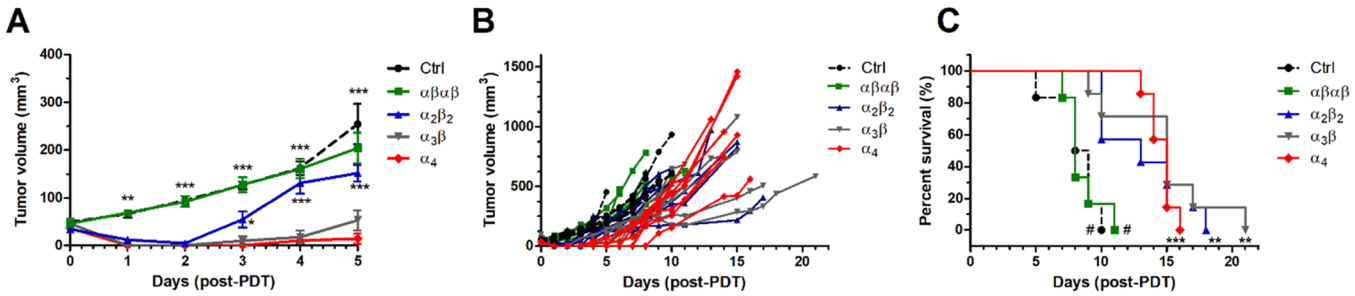

Figure 7. Cellular-PDT (DLI = 24 h) of female BALB/c mice bearing CT26 tumors with 0.35 mg/kg redaporfin atropisomers and 60 J/cm^2 at 750 nm. (A) Tumor volume represented as mean ± SEM 5 days post-PDT, which corresponds to the time interval where no mouse reached the humane endpoint; significance level vs the α_4 atropisomer was evaluated by two-way ANOVA. (B) Tumor volume for each individual mouse until the humane endpoint was reached. (C) Survival curves for treatment groups with 6−7 mice. The significance level between the different treated groups was evaluated by Log-rank (Mantel−Cox) test vs Ctrl (* $p < 0.05$, ** $p < 0.01$, and *** $p < 0.001$) or α_4 (# $p < 0.001$).

introduces very minor changes in the pattern of membrane interaction identified for redaporfin atropisomers.

Evaluated together, RP-HPLC retention times, differential phototoxicity, interaction with small quantities of liposomes, and cell uptake with the depletion of ATP indicate that differential redaporfin atropisomer internalization by cells is essentially a passive process and is strongly dependent on individual interactions between the atropisomer configuration and the phospholipid bilayer. Although redaporfin is a large molecule, cell uptake of its α_4 atropisomer is fast and efficient in vitro. In view of the lack of specificity of plasma proteins in cell uptake, varying atropisomer tumor uptake should also be observed in vivo.

In Vivo Tumor Accumulation of Atropisomers. The poor water solubility of redaporfin and P11 atropisomers required the use of Kolliphor EL-based formulations. We prepared a formulation similar to that in clinical use for redaporfin (atropisomer mixture), although a slightly higher Kolliphor EL content (0.5% v/v) was required for individual atropisomers relative to the 0.2% (v/v) used for the redaporfin mixture.[73] The isolated atropisomers were more difficult to solubilize than their mixture, probably because their crystal packing forces were stronger. A further increase of Kolliphor EL to 2% (v/v) was required to formulate P11 atropisomers as the porphyrins showed lower solubility. Although the Kolliphor EL content was different in these formulations, dynamic light scattering revealed that the micelles had similar relative sizes, ranging from 13 to 25 nm (Table S7). Studies of cellular internalization and phototoxicity conducted with redaporfin atropisomers formulated in Kolliphor EL maintained the differential uptake and phototoxicity profile previously described for the unformulated atropisomeric forms (Figure 6A,B). This suggests that the atropisomers are close to the surface of the micelles. The polar sulfonamide groups of α_4 are most likely orientated toward the micelle exterior, meaning that the interaction of the polar sulfonamide groups with the outer polar heads of the phospholipids of the cell's membrane is facilitated.

The differential accumulation of P11 atropisomers in vivo was studied following intravenous (i.v.) administration of the 2% (v/v) Kolliphor EL formulation in mice bearing CT26 subcutaneous tumors. P11 was studied as the uptake profile may be considered analogous, and bacteriochlorin atropisomers were maintained for therapeutic studies. This was followed, after appropriate times, by tumor excision and preparation of single cell suspensions which were submitted to P11 fluorescence detection by flow cytometry. We selected α_4 and $\alpha\beta\alpha\beta$ atropisomers for this comparison in view of their differences in vitro. The highest signal for both atropisomers was observed 24 h post-administration, although significant internalization was still detected at 72 h (Figure 6C). The internalization of α_4 by the tumor cells was over a factor of 2 higher than the internalization of $\alpha\beta\alpha\beta$. These observations are aligned with the results previously obtained in vitro, thus confirming the superiority of α_4 to penetrate across the cell membranes. The orientation of the aryl sulfonamide groups present in these conformers has significant implications in tumor cell uptake in vitro and in vivo. Next, we evaluated the therapeutic significance of differential cell uptake.

Impact of Differential Atropisomer Tumor Uptake on PDT Efficacy. PDT is well suited to evaluate the impact of differential atropisomer uptake by tumor cells because the drug-to-light interval (DLI) between the administration of the photosensitizer and the illumination of the target tissue determines whether the therapeutic effect results from ROS outside the cells (short DLI) or inside the cells (long DLI). At DLI = 15 min, the photosensitizer is activated in the vasculature, and this therapeutic approach is known as vascular-PDT.[74] However, using DLI = 24 h, the photosensitizer has time to be internalized by tumor cells, and this approach is named cellular-PDT.[59] In view of the data presented above, we do not expect an effect of differential atropisomer uptake in vascular-PDT, but, in cellular-PDT, α_4 should prove superior and $\alpha\beta\alpha\beta$ inferior to the other atropisomers.

Preliminary screening of drug and light doses to be used with DLI = 24 h led to the combination of 0.35 mg/kg of the α_4 redaporfin atropisomer with a light dose of 60 J/cm^2 to treat BALB/c female mice with subcutaneous CT26 tumors with a minimum diameter of 5 mm on the day of treatment. Higher drug doses were associated with lethality cases within 3 days of treatment. This combination was then applied with all atropisomers (Figures 7A−C and S16). Mice treated with the α_4 atropisomer showed the highest edema with undefined tumor boarders. 24 h post-treatment tumor necrosis was visible. No changes relative to the control (Crtl) group were observed with the $\alpha\beta\alpha\beta$ atropisomer, while $\alpha_2\beta_2$- and $\alpha_3\beta$-induced moderate edema and necrosis were present within the boundaries of the tumor 24−48 h post-PDT (Figure S16). The largest differences in the ability of atropisomers to control tumor growth were observed in the first 5 days post-treatment (Figure 7A,B). Although CT26 tumors regrew after cellular-PDT, overall survival times exhibited statistically significant differences. PDT with α_4 and $\alpha_3\beta$ atropisomers increased the

https://doi.org/10.1021/jacs.2c05844
J. Am. Chem. Soc. 2022, 144, 15252−15265

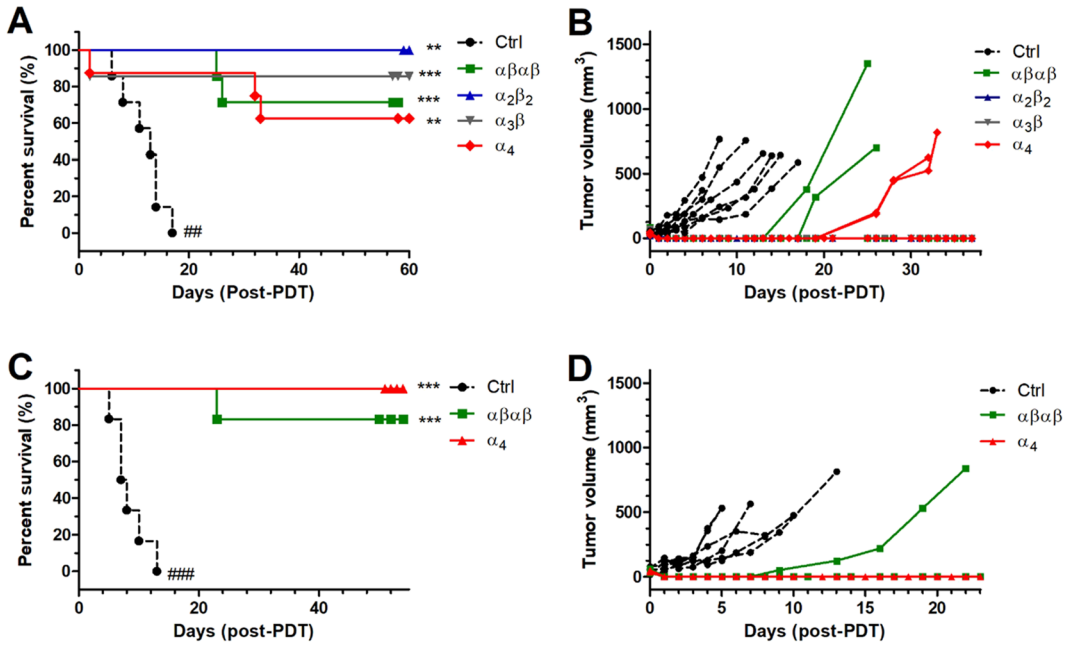

Figure 8. Vascular-PDT (DLI = 15 min) of BALB/c mice bearing CT26 tumors with 0.45 mg/kg redaporfin atropisomers and 40 J/cm^2 at 750 nm. (A) Survival curves for treatment groups with 6−8 female mice. (B) Tumor volume for each individual female mouse until the endpoint was reached. (C) Survival curves for treatment groups with 6 male mice. (D) Tumor volume for each individual male mouse until the endpoint was reached. The significance level between the different treated groups was evaluated by Log-rank (Mantel−Cox) test vs Ctrl (* $p < 0.05$, ** $p < 0.01$, and *** $p < 0.001$) or α_4 (## $p < 0.01$ and ### $p < 0.001$).

median survival to 15 days in comparison to the slightly lower improvement mediated by $\alpha_2\beta_2$ (13.5 days). In contrast, no improvement of the overall median survival was attained with the $\alpha\beta\alpha\beta$ (8 days) compared to that with the Ctrl group (8.5 days). Comparison of PDT efficacy for each individual atropisomer with the Ctrl group revealed the largest statistical significance for α_4 ($p = 0.0002$) which was in contrast to the $\alpha\beta\alpha\beta$ atropisomer ($p = 0.8549$). The p values of 0.0028 and 0.0017 were obtained for $\alpha_3\beta$ and $\alpha_2\beta_2$, respectively (Figure 7C). These results indicate that the orientation of aryl sulfonamide substituents in redaporfin atropisomers changes their internalization by cells of the tumor microenvironment and, consequently, alters cellular-PDT efficacy. Improved internalization and phototoxicity of the α_4 conformer were also observed in HaCat keratinocytes (Figure S17), which are the most abundant cell type in the skin epidermis. However, experiments carried out with a solar simulator demonstrated that the unspecific internalization of α_4 by normal skin cells was not associated with significantly exacerbated skin photosensitivity when compared to the redaporfin mixture (Figure S18). Notably, 7 days after i.v. administration of a therapeutic dose of α_4, 30 min exposure of depilated mice to a solar simulator equivalent to direct solar irradiation at noon in the US and Southern Europe did not elicit any measurable skin reaction.

Vascular-PDT of CT26 tumors with redaporfin shows much higher efficacy than cellular-PDT,[45,46] and the clinical translation of redaporfin for the treatment of advanced head and neck cancer employs vascular-PDT.[21] However, related, more lipophilic, photosensitizers demonstrate enhanced efficiency in cellular-PDT protocols.[59] Vascular-PDT produces a strong and selective destruction of the tumor blood vessels and is associated with extensive edema and necrosis.[45] In comparison, cellular-PDT facilitates optimal distribution of the compound in cellular compartments with therapeutic outcome dependent on photosensitizer cellular localization.[26] Screening of vascular-PDT in female BALB/c mice bearing implanted CT26 tumors with the α_4 atropisomer, using DLI = 15 min, led to the combination of 0.45 mg/kg with 40 J/cm^2 to obtain cures without significant lethality. This protocol was then applied to all atropisomers. Although conditions appeared safe when tested with a small number of mice ($n = 3$), vascular-PDT with α_4 and $\alpha_3\beta$ displayed lethality within the first 72 h of treatment, with the death of one animal from each group (included in the Kaplan−Meier analysis, Figure 8A). Cures (between 60 and 100%) were observed in all treatment groups. Tumors regrew in two animals of the $\alpha\beta\alpha\beta$ and α_4 groups. As anticipated, the overall impact of atropisomeric configuration on vascular-PDT efficacy was not statistically significant (Figure 8A,B). To confirm this result in the absence of lethality, male BALB/c mice bearing CT26 tumors were treated under the same conditions using $\alpha\beta\alpha\beta$ and α_4 atropisomers (Figure 8C,D). The higher weight of male BALB/c improved the tolerance to PDT when the same size tumors and drug and light doses were employed. We obtained 100% cures with male mice treated with α_4, while one mouse from the $\alpha\beta\alpha\beta$ group experienced tumor regrowth. This difference between α_4 and $\alpha\beta\alpha\beta$ groups was not statistically significant. Our vascular-PDT data confirm that the similarity of the photophysical and photochemical properties of the different atropisomers leads to similar therapeutic outcomes when the cellular uptake is not relevant. Combined with cellular-PDT, our results reveal the critical importance of enabling large molecules to attain their targets within cells.

Vascular-PDT with redaporfin triggers anti-tumor immunity with immunological memory.[45−47] We evaluated the immunological memory of mice (both female and male) cured with vascular-PDT using isolated atropisomers, from the experiments described above, by re-challenging the cured mice with CT26 cells 6 weeks post-PDT. Significant tumor rejections

https://doi.org/10.1021/jacs.2c05844
J. Am. Chem. Soc. 2022, 144, 15252−15265

were observed for all atropisomers without major differences between them (Figure S19). Immune response after vascular-PDT is not atropisomer-specific.

Implications for Cell Uptake of Macromolecules. One of the foundations of medicinal chemistry is that the strength of intermolecular interactions dictates the affinity of a drug to its target.[75,76] Atropisomers may show differential target selectivity because stable conformers could have different steric, hydrophobic, electrostatic, and H-bonding interactions with their targets. However, the pharmacological action of PDT is mediated by ROS, and these species are generated in a loose interaction between a photosensitizer molecule and molecular oxygen. Therefore, all atropisomers of a given photosensitizer are expected to have similar interactions with O_2, as shown in Table 1 for redaporfin atropisomers, and to have similar PDT efficacies. This is not the case when atropisomerism changes cell uptake and intracellular localization. Indeed, the first report on the photosensitizing ability of 5,10,15,20-tetrakis(*o*-acetamidophenyl)porphyrin atropisomers did not identify differences between atropisomers;[37] such differences became more evident later with more lipophilic 5,10,15,20-tetrakis(*o*-propionamidophenyl)-porphyrin atropisomers.[33] The photosensitizing abilities of the atropisomers of these "picket fence" porphyrins were correlated with their retention in silica gel, $\alpha_4 > \alpha_3\beta > \alpha_2\beta_2 > \alpha\beta\alpha\beta$, which was confirmed by this work, but the data were interpreted in terms of propensity for monomeric solubility in aqueous solution rather than on the basis of molecular topology.[33]

Various aspects of the properties of redaporfin atropisomers disclosed in this work are unexpected and support a new rationale to design the cellular uptake of large molecules. Specifically, redaporfin atropisomers show (i) the same order of retention times in silica gel and in RP-HPLC, $\alpha_4 > \alpha_3\beta > \alpha_2\beta_2 > \alpha\beta\alpha\beta$, a paradoxical result; (ii) that the order of $\mathrm{LogP_{OW}}$ values, $\alpha_3\beta > \alpha_4 > \alpha_2\beta_2 \approx \alpha\beta\alpha\beta$, correlates with the order of monomeric solubilization at large POPC concentrations and is a measure of lipophilicity; (iii) that the addition of hexane to a dichloromethane solution of atropisomers increases the fraction of α_4 in the less polar solvent mixture, which is a different measure of lipophilicity; and (iv) that atropisomer monomeric fluorescence at small POPC concentrations follows the order of cellular uptake, $\alpha_4 > \alpha_3\beta > \alpha_2\beta_2 > \alpha\beta\alpha\beta$. These results show that the four polar sulfonamide groups on the same side of the macrocycle do not cause α_4 to be the most polar atropisomer, as intuitively expected. Additionally, the higher solubility of α_4 in less polar solvent mixtures is not a simple display of lipophilicity. The differential solvation on the two sides of the macrocycle enhances the α_4 cell uptake in vivo and in vitro. Indeed, (i) the order of cellular uptake, $\alpha_4 > \alpha_3\beta > \alpha_2\beta_2 > \alpha\beta\alpha\beta$, is the same as the order of in vitro phototoxicity; (ii) depletion of ATP or the presence of plasma proteins has minimal effect on the cellular uptake; (iii) tumor uptake in vivo is larger for α_4 than for $\alpha\beta\alpha\beta$; and (iv) atropisomers with a higher cell uptake have enhanced photodynamic effect in cellular-PDT but not in vascular-PDT. Our results are consistent with cell uptake predominantly by passive diffusion through the cell membrane, which is much more efficient for the α_4 atropisomer and explains its higher phototoxicity in vitro and in cellular-PDT.

The best description for α_4 is that it is the most amphipathic atropisomer and is prone to locate at the interface between polar and lipophilic domains. This is consistent with the interfacial orientation adopted in micelles by α_4 atropisomers of short-chain picket-fence porphyrins, where the hydrophilic side chains point to the surrounding aqueous environment, whereas the porphyrin core is somewhat buried in the hydrophobic center.[77,78] Moreover, the X-ray structure of α_4 P11 reveals a saddle deformation of its macrocycle, possibly driven by steric interactions between the polar groups, and a preference for a three-dimensional hydrogen-bonded network with disordered acetonitrile (solvate) molecules. This suggests that the energy penalty for desolvation in the transition between aqueous media to membranes is lower for α_4 than for the other atropisomers.

Our data uncovers the importance of spatial orientation of aryl methylsufonamide groups in the cellular uptake of large molecules. The topology of α_4 points 8 H-bond acceptors and 4 H-bond donors to the same side of the macrocycle and facilitates hydrogen bonding with the silanol groups on the silica surface or with the phosphate groups of membrane phospholipids. However, the lipophilicity of α_4 causes higher retentions in RP-HPLC and facilitates monomeric solubilization in membranes (Figure S20A). This suggests a cell uptake mechanism where H-bonding promotes the transfer of α_4 from water:DMSO 99.96:0.04 (or from 2% (v/v) Kolliphor EL micelles or plasma proteins) to the surface of membranes; then, α_4 flips to accommodate its lipophilic moiety inside the membrane and eventually finds its way to the interior of the cell. This bind-flip mechanism of cell uptake is made possible by amphipathicity and facilitated desolvation (Figure S20B). The topology of aryl methylsulfonamides in α_4 is a cell-penetrating motif for large molecules.

It is interesting to compare the topology of α_4 with that of cyclosporine (MW = 1203 Da), which is a rare example of a large molecule that efficiently crosses cell membranes by passive diffusion.[79] N^{α}-Methylation of the cyclosporine backbone amides reduces the number of H-bond donors to 5 and intramolecular H-bonding lowers its desolvation energy. Cyclosporine is in an "open" conformation in aqueous solutions, which allows amides to interact with cell membranes via hydrogen bonds. However, it changes to a "closed" conformation in the lipid bilayer, making use of intramolecular hydrogen bonding to decrease its polarity.[79,80] The α_4 atropisomer redaporfin also offers favorable H-bonding with the cell surface and uses amphipathicity to flip the macromolecule into the cell membrane at a lower desolvation energy cost.

The activation of a drug with light is an intrinsic property of PDT which allows for the study of pharmacodynamics with spatiotemporal control. We studied the pharmacodynamics of atropisomers before they had time to be internalized by cells (vascular-PDT) and after cellular uptake (cellular-PDT). Redaporfin atropisomers exhibited differential pharmacodynamics in cellular-PDT, providing evidence that a specific topology of aryl methylsufonamide substituents can work as a cell-penetrating motif in vivo. The implications of this finding for the design of macromolecule cytosolic delivery should not obscure the remarkable achievement of 100% cures of BALB/c mice with subcutaneous tumors in one single vascular-PDT treatment.

CONCLUSIONS

In summary, we show that atropisomers of *meso*-tetraarylporphyrin derivatives with fluorine atoms in the *ortho* positions of the aryl rings and a sulfonamide group in the *meta* position are

https://doi.org/10.1021/jacs.2c05844
J. Am. Chem. Soc. 2022, 144, 15252−15265

separable by flash chromatography and very stable at room temperature. The rotamer with four sulfonamide groups on the same side of the macrocycle, that is, the α_4 atropisomer, has enhanced ability to access the cellular membrane and diffuse to the cytosol. Efficient cytosolic delivery by passive diffusion of molecules as large as redaporfin is rare and substantial increase of such delivery by rotation of C−C single bonds is entirely unexpected. The α_4 atropisomer exhibits surfactant properties, in which the macrocycle is likely orientated toward lipophilic domains and the arylsulfonamides exposed to the polar environment. This favors H-binding of the four sulfonamide groups with sulfates and carboxylates of the cell membrane. The enhanced amphipathic character of the α_4 atropisomer offers the opportunity for a flip of its lipophilic side to the interior of the membrane with lower desolvation costs than the other atropisomers. Most importantly, the seamless α_4 cell internalization observed in vitro could be transferred to an animal model relevant in oncology. Vascular-PDT with separated redaporfin atropisomers achieved 100% cure rates in tumor-bearing animal models. The differential pharmacodynamics of redaporfin atropisomers are a new example of the far-reaching consequences of atropisomerism in biological activity and drug action. They suggest a new design of cell-penetrating motifs which demonstrate impact in vivo.

■ ASSOCIATED CONTENT

Supporting Information

The Supporting Information is available free of charge at https://pubs.acs.org/doi/10.1021/jacs.2c05844.

Experimental section, additional figures, and tables (PDF)

Accession Codes

CCDC 2124975−2124976 contain the supplementary crystallographic data for this paper. These data can be obtained free of charge via www.ccdc.cam.ac.uk/data_request/cif, or by emailing data_request@ccdc.cam.ac.uk, or by contacting The Cambridge Crystallographic Data Centre, 12 Union Road, Cambridge CB2 1EZ, UK; fax: +44 1223 336033.

■ AUTHOR INFORMATION

Corresponding Authors

Lígia C. Gomes-da-Silva − *CQC, Coimbra Chemistry Center, University of Coimbra, Coimbra 3004-535, Portugal;* orcid.org/0000-0003-0624-8819; Email: ligia.silva@uc.pt

Luis G. Arnaut − *CQC, Coimbra Chemistry Center, University of Coimbra, Coimbra 3004-535, Portugal;* orcid.org/0000-0002-3223-4819; Email: lgarnaut@ci.uc.pt

Authors

Claire Donohoe − *CQC, Coimbra Chemistry Center, University of Coimbra, Coimbra 3004-535, Portugal; Medicinal Chemistry, Trinity Translational Medicine Institute, Trinity Centre for Health Sciences, St. James's Hospital, Trinity College Dublin, The University of Dublin, Dublin 8, Ireland*

Fábio A. Schaberle − *CQC, Coimbra Chemistry Center, University of Coimbra, Coimbra 3004-535, Portugal;* orcid.org/0000-0002-9339-7259

Fábio M. S. Rodrigues − *CQC, Coimbra Chemistry Center, University of Coimbra, Coimbra 3004-535, Portugal;* orcid.org/0000-0002-1085-2720

Nuno P. F. Gonçalves − *Luzitin SA, Ed. Bluepharma, S. Martinho do Bispo, Coimbra 3045-016, Portugal;* Present Address: Department of Chemistry, Universidade de Aveiro, 3810-193 Aveiro, Portugal (N.P.F.G.)

Christopher J. Kingsbury − *School of Chemistry, Chair of Organic Chemistry, Trinity Biomedical Sciences Institute, Trinity College Dublin, The University of Dublin, Dublin 2, Ireland*

Mariette M. Pereira − *CQC, Coimbra Chemistry Center, University of Coimbra, Coimbra 3004-535, Portugal;* orcid.org/0000-0003-4958-7677

Mathias O. Senge − *Medicinal Chemistry, Trinity Translational Medicine Institute, Trinity Centre for Health Sciences, St. James's Hospital, Trinity College Dublin, The University of Dublin, Dublin 8, Ireland; Institute for Advanced Study (TUM-IAS), Technical University of Munich, Garching 85748, Germany;* orcid.org/0000-0002-7467-1654

Complete contact information is available at: https://pubs.acs.org/10.1021/jacs.2c05844

Funding

This project has received funding from the European Union's Horizon 2020 research and innovation program under the Marie Sklodowska-Curie grant agreement number 764837 (Polythea—How light can save lives), the Portuguese Foundation for Science and Technology (UID/QUI/00313/2019 and PTDC/QUI-OUT/0303/2021), the European Innovation Council through the FET-OPEN Project INITIO (Grant Agreement: 828779), and the Technical University of Munich—Institute for Advanced Study through a Hans Fischer Senior Fellowship (M.O.S.). This work was supported by the Higher Education Authority and the Department of Further and Higher Education, Research, Innovation and Science (Ireland).

Notes

The authors declare the following competing financial interest(s): F.S., N.G., M.P., and L.G.A. have patents on redaporfin licensed to Luzitin SA. N.G. was an employee of Luzitin and is now an independent researcher at the University of Aveiro.

■ ACKNOWLEDGMENTS

The authors thank Prof. Maria João Moreno for providing liposomes; Prof. Guido Kroemer for the donation of U-2 OS cells expressing CALR-GFP or GALT1-GFP; Karolis Novaiša for project discussion; and Catarina Pinto, Luísa Cortes, and Ana-Clara B. Rodrigues for providing technical assistance with HPLC, confocal microscopy, and fluorescence spectroscopy, respectively.

■ REFERENCES

(1) Sakamoto, K.; Michibata, J.; Hirai, Y.; Ide, A.; Ikitoh, A.; Takatani-Nakase, T.; Futaki, S. Potentiating the Membrane Interaction of an Attenuated Cationic Amphiphilic Lytic Peptide for Intracellular Protein Delivery by Anchoring with Pyrene Moiety. *Bioconjugate Chem.* **2021**, *32*, 950−957.

(2) McKinlay, C. J.; Waymouth, R. M.; Wender, P. A. Cell-Penetrating, Guanidinium-Rich Oligophosphoesters: Effective and Versatile Molecular Transporters for Drug and Probe Delivery. *J. Am. Chem. Soc.* **2016**, *138*, 3510−3517.

(3) Pei, D.; Buyanova, M. Overcoming Endosomal Entrapment in Drug Delivery. *Bioconjate Chem.* **2019**, *30*, 273−283.

(4) Guha, S.; Ghimire, J.; Wu, E.; Wimley, W. C. Mechanistic Landscape of Membrane-Permeabilizing Peptides. *Chem. Rev.* **2019**, *119*, 6040−6085.
(5) Allen, J.; Najjar, K.; Erazo-Oliveras, A.; Kondow-McConaghy, H. M.; Brock, D. J.; Graham, K.; Hager, E. C.; Marschall, A. L. J.; Dübel, S.; Juliano, R. L.; Pellois, J.-P. Cytosolic Delivery of Macromolecules in Live Human Cells Using the Combined Endosomal Escape Activities of a Small Molecule and Cell Penetrating Peptides. *ACS Chem. Biol.* **2019**, *14*, 2641−2651.
(6) López-Andarias, J.; Saarbach, J.; Moreau, D.; Cheng, Y.; Derivery, E.; Laurent, Q.; González-Gaitán, M.; Winssinger, N.; Sakai, N.; Matile, S. Cell-Penetrating Streptavidin: A General Tool for Bifunctional Delivery with Spatiotemporal Control, Mediated by Transport Systems Such as Adaptive Benzopolysulfane Networks. *J. Am. Chem. Soc.* **2020**, *142*, 4784−4792.
(7) Pulcu, G. S.; Galenkamp, N. S.; Qing, Y.; Gasparini, G.; Mikhailova, E.; Matile, S.; Bayley, H. Single-Molecule Kinetics of Growth and Degradation of Cell-Penetrating Poly(disulfide)s. *J. Am. Chem. Soc.* **2019**, *141*, 12444−12447.
(8) Kelly, C. N.; Townsend, C. E.; Jain, A. N.; Naylor, M. R.; Pye, C. R.; Schwochert, J.; Lokey, R. S. Geometrically Diverse Lariat Peptide Scaffolds Reveal an Untapped Chemical Space of High Membrane Permeability. *J. Am. Chem. Soc.* **2021**, *143*, 705−714.
(9) Kubi, G. A.; Qian, Z.; Amiar, S.; Sahni, A.; Stahelin, R. V.; Pei, D. Non-Peptidic Cell-Penetrating Motifs for Mitochondrion-Specific Cargo Delivery. *Angew. Chem., Int. Ed.* **2018**, *57*, 17183−17188.
(10) Vinogradov, A. A.; Yin, Y.; Suga, H. Macrocyclic Peptides as Drug Candidates: Recent Progress and Remaining Challenges. *J. Am. Chem. Soc.* **2019**, *141*, 4167−4181.
(11) Barlow, N.; Chalmers, D. K.; Williams-Noonan, B. J.; Thompson, P. E.; Norton, R. S. Improving Membrane Permeation in the Beyond Rule-of-Five Space by Using Prodrugs to Mask Hydrogen Bond Donors. *ACS Chem. Biol.* **2020**, *15*, 2070−2078.
(12) Gao, Y.-H.; Lovreković, V.; Kussayeva, A.; Chen, D.-Y.; Margetić, D.; Chen, Z.-L. The photodynamic activities of dimethyl 131-[2-(guanidinyl)ethylamino] chlorin e6 photosensitizers in A549 tumor. *Eur. J. Med. Chem.* **2019**, *177*, 144−152.
(13) Sibrian-Vazquez, M.; Nesterova, I. V.; Jensen, T. J.; Vicente, M. G. H. Mitochondria Targeting by Guanidine− and Biguanidine−Porphyrin Photosensitizers. *Bioconjugate Chem.* **2008**, *19*, 705−713.
(14) Clayden, J.; Moran, W. J.; Edwards, P. J.; LaPlante, S. R. The Challenge of Atropisomerism in Drug Discovery. *Angew. Chem., Int. Ed.* **2009**, *48*, 6398−6401.
(15) LaPlante, S. R.; Edwards, P. J.; Fader, L. D.; Jakalian, A.; Hucke, O. Revealing Atropisomer Axial Chirality in Drug Discovery. *ChemMedChem* **2011**, *6*, 505−513.
(16) Smyth, J. E.; Butler, N. M.; Keller, P. A. A twist of nature − the significance of atropisomers in biological systems. *Nat. Prod. Rep.* **2015**, *32*, 1562−1583.
(17) Glunz, P. W. Recent encounters with atropisomerism in drug discovery. *Bioorg. Med. Chem. Lett.* **2018**, *28*, 53−60.
(18) Toenjes, S. T.; Gustafson, J. L. Atropisomerism in medicinal chemistry: challenges and opportunities. *Future Med. Chem.* **2018**, *10*, 409−422.
(19) Mancinelli, M.; Bencivenni, G.; Pecorari, D.; Mazzanti, A. Stereochemistry and Recent Applications of Axially Chiral Organic Molecules. *Eur. J. Org. Chem.* **2020**, 4070−4086.
(20) Smith, D. E.; Marquez, I.; Lokensgard, M. E.; Rheingold, A. L.; Hecht, D. A.; Gustafson, J. L. Exploiting Atropisomerism to Increase the Target Selectivity of Kinase Inhibitors. *Angew. Chem., Int. Ed.* **2015**, *54*, 11754−11759.
(21) Santos, L. L.; Oliveira, J.; Monteiro, E.; Santos, J.; Sarmento, C. Treatment of Head and Neck Cancer with Photodynamic Therapy with Redaporfin: A Clinical Case Report. *Case Rep. Oncol.* **2018**, *11*, 769−776.
(22) Callaghan, S.; Senge, M. O. The good, the bad, and the ugly − controlling singlet oxygen through design of photosensitizers and delivery systems for photodynamic therapy. *Photochem. Photobiol. Sci.* **2018**, *17*, 1490−1514.
(23) Dąbrowski, J. M.; Arnaut, L. G. Photodynamic therapy (PDT) of cancer: from local to systemic treatment. *Photochem. Photobiol. Sci.* **2015**, *14*, 1765−1780.
(24) Agostinis, P.; Berg, K.; Cengel, K. A.; Foster, T. H.; Girotti, A. W.; Gollnick, S. O.; Hahn, S. M.; Hamblin, M. R.; Juzeniene, A.; Kessel, D.; Korbelik, M.; Moan, J.; Mroz, P.; Nowis, D.; Piette, J.; Wilson, B. C.; Golab, J. Photodynamic therapy of cancer: an update. *Ca-Cancer J. Clin.* **2011**, *61*, 250−281.
(25) Celli, J. P.; Spring, B. Q.; Rizvi, I.; Evans, C. L.; Samkoe, K. S.; Verma, S.; Pogue, B. W.; Hasan, T. Imaging and photodynamic therapy: mechanisms, monitoring, and optimization. *Chem. Rev.* **2010**, *110*, 2795−2838.
(26) Donohoe, C.; Senge, M. O.; Arnaut, L. G.; Gomes-da-Silva, L. C. Cell death in photodynamic therapy: From oxidative stress to anti-tumor immunity. *Biochim. Biophys. Acta, Rev. Cancer* **2019**, *1872*, 188308.
(27) Bonnett, R. Photosensitizers of the porphyrin and phthalocyanine series for photodynamic therapy. *Chem. Soc. Rev.* **1995**, *24*, 19−33.
(28) Frochot, C.; Mordon, S. Update of the situation of clinical photodynamic therapy in Europe in the 2003−2018 period. *J. Porphyrins Phthalocyanines* **2019**, *23*, 347−357.
(29) Lindsey, J. S.; Schreiman, I. C.; Hsu, H. C.; Kearney, P. C.; Marguerettaz, A. M. Rothemund and Adler-Longo reactions revisited: synthesis of tetraphenylporphyrins under equilibrium conditions. *J. Org. Chem.* **1987**, *52*, 827−836.
(30) d'A Rocha Gonsalves, A. M.; Varejão, J. M. T. B.; Pereira, M. M. Some new aspects related to the synthesis of meso-substituted porphyrins. *J. Heterocycl. Chem.* **1991**, *28*, 635−640.
(31) Tomé, A. C.; Silva, A. M. S.; Alkorta, I.; Elguero, J. Atropisomerism and conformational aspects of meso-tetraarylporphyrins and related compounds. *J. Porphyrins Phthalocyanines* **2011**, *15*, 1−28.
(32) Collman, J. P.; Gagne, R. R.; Reed, C.; Halbert, T. R.; Lang, G.; Robinson, W. T. Picket fence porphyrins. Synthetic models for oxygen binding hemoproteins. *J. Am. Chem. Soc.* **1975**, *97*, 1427−1439.
(33) Barber, D. C.; VanDerMeid, K. R.; Gibson, S. L.; Hilf, R.; Whitten, D. G. Photosensitizing activities of picket fence porphyrins *in vitro* and *in vivo*. *Cancer Res.* **1991**, *51*, 1836−1845.
(34) Ressurreição, A. S. M.; Pineiro, M.; Arnaut, L. G.; d'A Rocha Gonsalves, A. M. Atropisomers of 5,10,15,20-tetrakis(2,6-dichloro-3-sulfamoyl-phenyl)porphyrins. *J. Porphyrins Phthalocyanines* **2007**, *11*, 50−57.
(35) Norvaiša, K.; O'Brien, J. E.; Gibbons, D. J.; Senge, M. O. Elucidating Atropisomerism in Nonplanar Porphyrins with Tunable Supramolecular Complexes. *Chem. − Eur. J.* **2021**, *27*, 331−339.
(36) Zhu, L.; Himmel, L.; Merkes, J. M.; Kiessling, F.; Rueping, M.; Banala, S. Atropisomers of meso Tetra(N-Mesyl Pyrrol-2-yl) Porphyrins: Synthesis, Isolation and Characterization of All-Pyrrolic Porphyrins. *Chem. − Eur. J.* **2020**, *26*, 4232−4235.
(37) Hagan, W. J., Jr.; Barber, D. C.; Whitten, D. G.; Kelly, M.; Albrecht, F.; Gibson, S. L.; Hilf, R. Picket-fence porphyrins as potential phototherapeutic agents. *Cancer Res.* **1988**, *48*, 1148−1152.
(38) Arnaut, L. Transitions between electronic states. In *Chemical Kinetics*, 2nd ed.; Arnaut, L., Ed.; Elsevier, 2021; pp 463−521.
(39) Richter, A. M.; Jain, A. K.; Canaan, A. J.; Waterfield, E.; Sternberg, E. D.; Levy, J. G. Photosensitizing efficiency of two regioisomers of the benzoporphyrin derivative monoacid ring a (BPD-MA). *Biochem. Pharmacol.* **1992**, *43*, 2349−2358.
(40) Tasso, T. T.; Tsubone, T. M.; Baptista, M. S.; Mattiazzi, L. M.; Acunha, T. V.; Iglesias, B. A. Isomeric effect on the properties of tetraplatinated porphyrins showing optimized phototoxicity for photodynamic therapy. *Dalton Trans.* **2017**, *46*, 11037−11045.
(41) Feng, X.; Shi, Y.; Xie, L.; Zhang, K.; Wang, X.; Liu, Q.; Wang, P. Synthesis, Characterization, and Biological Evaluation of a Porphyrin-Based Photosensitizer and Its Isomer for Effective Photodynamic Therapy against Breast Cancer. *J. Med. Chem.* **2018**, *61*, 7189−7201.

https://doi.org/10.1021/jacs.2c05844
J. Am. Chem. Soc. 2022, 144, 15252−15265

(42) Pereira, M. M.; Abreu, A. R.; Goncalves, N. P. F.; Calvete, M. J. F.; Simões, A. V. C.; Monteiro, C. J. P.; Arnaut, L. G.; Eusébio, M. E.; Canotilho, J. An insight into solvent-free diimide porphyrin reduction: a versatile approach for meso-aryl hydroporphyrin synthesis. *Green Chem.* **2012**, *14*, 1666−1672.
(43) Arnaut, L. G.; Pereira, M. M.; Dąbrowski, J. M.; Silva, E. F. F.; Schaberle, F. A.; Abreu, A. R.; Rocha, L. B.; Barsan, M. M.; Urbańska, K.; Stochel, G.; Brett, C. M. A. Photodynamic Therapy Efficacy Enhanced by Dynamics: The Role of Charge Transfer and Photostability in the Selection of Photosensitizers. *Chem. − Eur. J.* **2014**, *20*, 5346−5357.
(44) Soares, H. T.; Campos, J. R.; Gomes-da-Silva, L. C.; Schaberle, F. A.; Dabrowski, J. M.; Arnaut, L. G. Pro-oxidant and Antioxidant Effects in Photodynamic Therapy: Cells Recognise that Not All Exogenous ROS Are Alike. *ChemBioChem* **2016**, *17*, 836−842.
(45) Rocha, L. B.; Gomes-da-Silva, L. C.; Dąbrowski, J. M.; Arnaut, L. G. Elimination of primary tumours and control of metastasis with rationally designed bacteriochlorin photodynamic therapy regimens. *Eur. J. Cancer* **2015**, *51*, 1822−1830.
(46) Pucelik, B.; Arnaut, L. G.; Stochel, G.; Dąbrowski, J. M. Design of Pluronic-Based Formulation for Enhanced Redaporfin-Photodynamic Therapy against Pigmented Melanoma. *ACS Appl. Mater. Interfaces* **2016**, *8*, 22039−22055.
(47) Lobo, A. C. S.; Gomes-da-Silva, L. C.; Rodrigues-Santos, P.; Cabrita, A.; Santos-Rosa, M.; Arnaut, L. G. Immune Responses after Vascular Photodynamic Therapy with Redaporfin. *J. Clin. Med.* **2019**, *9*, 104−119.
(48) Karwicka, M.; Pucelik, B.; Gonet, M.; Elas, M.; Dąbrowski, J. M. Effects of Photodynamic Therapy with Redaporfin on Tumor Oxygenation and Blood Flow in a Lung Cancer Mouse Model. *Sci. Rep.* **2019**, *9*, 12655.
(49) Krzykawska-Serda, M.; Dąbrowski, J. M.; Arnaut, L. G.; Szczygieł, M.; Urbańska, K.; Stochel, G.; Elas, M. The role of strong hypoxia in tumors after treatment in the outcome of bacteriochlorin-based photodynamic therapy. *Free Radical Biol. Med.* **2014**, *73*, 239−251.
(50) Martin, D. J.; Mercado, B. Q.; Mayer, J. M. All Four Atropisomers of Iron Tetra(o-N,N,N-trimethylanilinium)porphyrin in Both the Ferric and Ferrous States. *Inorg. Chem.* **2021**, *60*, 5240−5251.
(51) Goncalves, N. P. F.; Santos, T. P. C. M.; Costa, G. P. N.; Monteiro, C. J. P.; Shaberle, F.; Alfar, S. C.; Abreu, A. C. R.; Pereira, M. M.; Arnaut, L. G. Atropisomers of Halogenated Tetraphenylbacteriochlorins and Chlorins and their use in Photodynamic Therapy. WO2016151458A1, September 29, 2016.
(52) Welerowicz, T.; Buszewski, B. The effect of stationary phase on lipophilicity determination of β-blockers using reverse-phase chromatographic systems. *Biomed. Chromatogr.* **2005**, *19*, 725−736.
(53) Spek, A. PLATON SQUEEZE: a tool for the calculation of the disordered solvent contribution to the calculated structure factors. *Acta Crystallogr., Sect. C: Struct. Chem.* **2015**, *71*, 9−18.
(54) Kingsbury, C. J.; Senge, M. O. The shape of porphyrins. *Coord. Chem. Rev.* **2021**, *431*, No. 213760.
(55) Houborg, K.; Harris, P.; Petersen, J.; Rowland, P.; Poulsen, J. C.; Schneider, P.; Vind, J.; Larsen, S. Impact of the physical and chemical environment on the molecular structure of Coprinus cinereus peroxidase. *Acta Crystallogr., Sect. D: Biol. Crystallogr.* **2003**, *59*, 989−996.
(56) Gomes-da-Silva, L. C.; Zhao, L.; Bezu, L.; Zhou, H.; Sauvat, A.; Liu, P.; Durand, S.; Leduc, M.; Souquere, S.; Loos, F.; Mondragón, L.; Sveinbjørnsson, B.; Rekdal, Ø.; Boncompain, G.; Perez, F.; Arnaut, L. G.; Kepp, O.; Kroemer, G. Photodynamic therapy with redaporfin targets the endoplasmic reticulum and Golgi apparatus. *EMBO J.* **2018**, *37*, No. e98354.
(57) Gomes-da-Silva, L. C.; Zhao, L.; Arnaut, L. G.; Kroemer, G.; Kepp, O. Redaporfin induces immunogenic cell death by selective destruction of the endoplasmic reticulum and the Golgi apparatus. *Oncotarget* **2018**, *9*, 31169−31170.
(58) Sugano, K.; Kansy, M.; Artursson, P.; Avdeef, A.; Bendels, S.; Di, L.; Ecker, G. F.; Faller, B.; Fischer, H.; Gerebtzoff, G.; Lennernaes, H.; Senner, F. Coexistence of passive and carrier-mediated processes in drug transport. *Nat. Rev. Drug Discovery* **2010**, *9*, 597−614.
(59) Pucelik, B.; Arnaut, L. G.; Dąbrowski, J. M. Lipophilicity of Bacteriochlorin-Based Photosensitizers as a Determinant for PDT Optimization through the Modulation of the Inflammatory Mediators. *J. Clin. Med.* **2019**, *9*, 8−34.
(60) Ricchelli, F. Photophysical properties of porphyrins in biological membranes. *J. Photochem. Photobiol., B* **1995**, *29*, 109−118.
(61) Ben-Dror, S.; Bronshtein, I.; Wiehe, A.; Röder, B.; Senge, M. O.; Ehrenberg, B. On the correlation between hydrophobicity, liposome binding and cellular uptake of porphyrin sensitizers. *Photochem. Photobiol.* **2006**, *82*, 695−701.
(62) Uchoa, A. F.; de Oliveira, K. T.; Baptista, M. S.; Bortoluzzi, A. J.; Iamamoto, Y.; Serra, O. A. Chlorin Photosensitizers Sterically Designed To Prevent Self-Aggregation. *J. Org. Chem.* **2011**, *76*, 8824−8832.
(63) Kelbauskas, L.; Dietel, W. Internalization of Aggregated Photosensitizers by Tumor Cells: Subcellular Time-resolved Fluorescence Spectroscopy on Derivatives of Pyropheophorbide-a Ethers and Chlorin e6 under Femtosecond One- and Two-photon Excitation. *Photochem. Photobiol.* **2002**, *76*, 686−694.
(64) Tomoda, H.; Kishimoto, Y.; Lee, Y. C. Temperature effect on endocytosis and exocytosis by rabbit alveolar macrophages. *J. Biol. Chem.* **1989**, *264*, 15445−15450.
(65) Mix, K. A.; Lomax, J. E.; Raines, R. T. Cytosolic Delivery of Proteins by Bioreversible Esterification. *J. Am. Chem. Soc.* **2017**, *139*, 14396−14398.
(66) Gunn, M. D.; Sen, A.; Chang, A.; Willerson, J. T.; Buja, L. M.; Chien, K. R. Mechanisms of accumulation of arachidonic acid in cultured myocardial cells during ATP depletion. *Am. J. Physiol.: Cell Physiol.* **1985**, *249*, H1188−H1194.
(67) Trimble, W. S.; Grinstein, S. Barriers to the free diffusion of proteins and lipids in the plasma membrane. *J. Cell. Biol.* **2015**, *208*, 259−271.
(68) Ricchelli, F.; Jori, G.; Gobbo, S.; Tronchin, M. Liposomes as models to study the distribution of porphyrins in cell membranes. *Biochim. Biophys. Acta, Biomembr.* **1991**, *1065*, 42−48.
(69) Korbelik, M.; Hung, J.; Lam, S.; Palcic, B. The effects of low density lipoproteins on uptake of Photofrin II. *Photochem. Photobiol.* **1990**, *51*, 191−196.
(70) Michael-Titus, A. T.; Whelpton, R.; Yaqub, Z. Binding of temoporfin to the lipoprotein fractions of human serum. *Br. J. Clin. Pharmacol.* **1995**, *40*, 594−597.
(71) Gierlich, P.; Mata, A. I.; Donohoe, C.; Brito, R. M. M.; Senge, M. O.; Gomes-da-Silva, L. C. Ligand-Targeted Delivery of Photosensitizers for Cancer Treatment. *Molecules* **2020**, *25*, 5317−5371.
(72) Mazor, O.; Brandis, A.; Plaks, V.; Neumark, E.; Rosenbach-Belkin, V.; Salomon, Y.; Scherz, A. WST11, a novel water-soluble bacteriochlorophyll derivative; cellular uptake, pharmacokinetics, biodistribution and vascular-targeted photodynamic activity using melanoma tumors as a model. *Photochem. Photobiol.* **2005**, *81*, 342−351.
(73) Saavedra, R.; Rocha, L. B.; Dąbrowski, J. M.; Arnaut, L. G. Modulation of biodistribution, pharmacokinetics, and photosensitivity with the delivery vehicle of a bacteriochlorin photosensitizer for photodynamic therapy. *ChemMedChem* **2014**, *9*, 390−398.
(74) Krammer, B. Vascular effects of photodynamic therapy. *Anticancer Res.* **2001**, *21*, 4271−4277.
(75) Ariens, E. J.; De Groot, W. M. Affinity and intrinsic-activity in the theory of competitive inhibition. III. Homologous decamethonium-derivatives and succinyl-choline-esters. *Arch. Int. Pharmacodyn. Ther.* **1954**, *99*, 193−205.
(76) Bissantz, C.; Kuhn, B.; Stahl, M. A. Medicinal Chemist's Guide to Molecular Interactions. *J. Med. Chem.* **2010**, *53*, 5061−5084.
(77) Collins-Gold, L. C.; Barber, D. C.; Hagan, W. J.; Gibson, S. L.; Hilf, R.; Whitten, D. G. Synthetic porphyrins at interfaces; photosensitization and related reactions of atropisomers of o-

https://doi.org/10.1021/jacs.2c05844
J. Am. Chem. Soc. 2022, 144, 15252−15265

substituted tetraphenylporphine derivatives in films, reversed micelles and membranes. *Photochem. Photobiol.* **1988**, *48*, 165−175.
(78) Barber, D. C.; Woodhouse, T. E.; Whitten, D. G. Diverse reactivities of picket fence porphyrin atropisomers in organized media: a probe of molecular location and orientation. *J. Phys. Chem.* **1992**, *96*, 5106−5114.
(79) Dougherty, P. G.; Sahni, A.; Pei, D. Understanding Cell Penetration of Cyclic Peptides. *Chem. Rev.* **2019**, *119*, 10241−10287.
(80) Wang, C. K.; Swedberg, J. E.; Harvey, P. J.; Kaas, Q.; Craik, D. J. Conformational Flexibility Is a Determinant of Permeability for Cyclosporin. *J. Phys. Chem. B* **2018**, *122*, 2261−2276.

https://doi.org/10.1021/jacs.2c05844
J. Am. Chem. Soc. 2022, 144, 15252−15265